Electronic Supplementary Material (ESI) for Journal of Materials Chemistry C.
This journal is © The Royal Society of Chemistry 2022

Nanosheet Molding Method to Estimate the Size of Bilayers Suspended in Liquid

Koki Sasaki, Jose A. Hernandez Gaitan, Yuki Tokuda, Koji Miyake, Yoshiaki Uchida,* and Norikazu Nishiyama

Graduate School of Engineering Science, Osaka University, 1-3 Machikaneyama-cho, Toyonaka, Osaka 560-8531, Japan

Supporting Information

Table of Contents

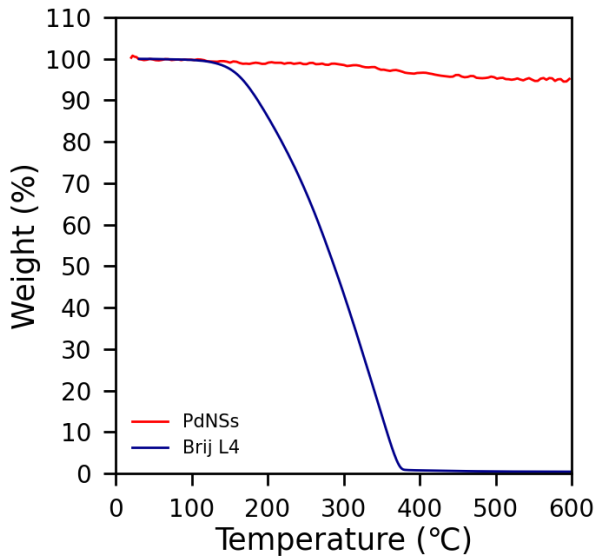

Fig. S1 Thermogravimetric analysis curve of PdNSs. Red and blue lines denote the data for the synthesized PdNSs and Brij L4, respectively.

Table S1 XRD peak positions and full widths at half-maximum for PdNSs and Pd fine particles.

Peak (2θ)	Full Width at Half Maximum (°)	
	Nanosheets	Fine particles
40.09	1.420	1.390
46.80	1.786	1.835
68.08	1.820	2.150
82.21	1.959	2.274

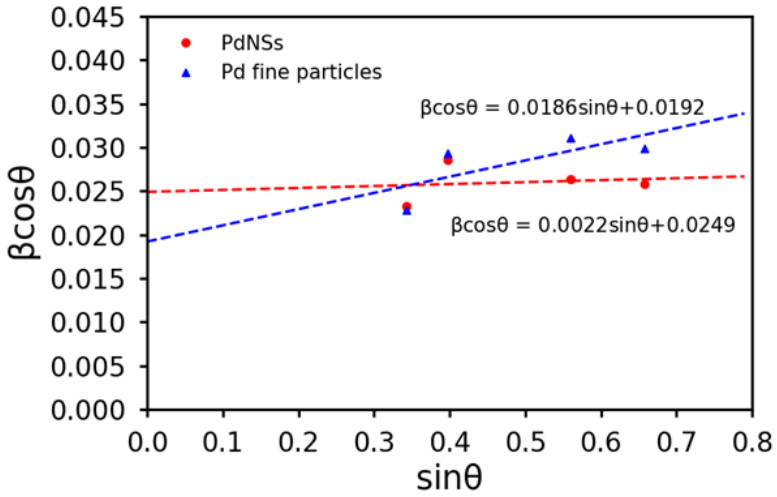

Fig. S2 Williamson-Hall plots for PdNSs and Pd fine particles. In the equations, β is full width at half-maximum, η is internal strain, *K* is Scherrer constant, λ is the X-ray wavelength, and *D* is crystallite size. The Scherrer constant used was 0.94 for cubic symmetry. The estimated *D* for PdNSs and Pd fine particles are 5.8 nm and 7.5 nm, respectively.

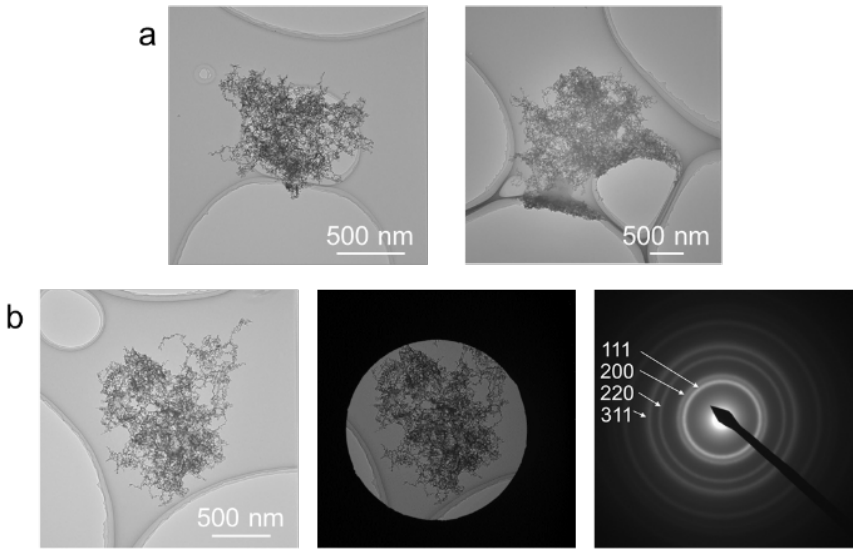

Fig. S3 TEM photographs and SAED pattern of PdNSs. (a) TEM photographs and (b) SAED pattern.

Table S2 Synthetic condition dependence of the size of PdNSs.

Product	w_{Me} / wt%	Width / nm	Thickness / nm
1	0	223 ± 53	8.30 ± 4.56
2	0.17	122 ± 18	3.31 ± 0.56
3	0.40	146 ± 31	3.44 ± 0.94
4	0.77	189 ± 41	2.80 ± 0.93
5	0.87	295 ± 55	1.86 ± 0.42
6	1.00	485 ± 65	2.18 ± 0.40
7	1.33	868 ± 208	2.36 ± 0.59
8	1.46	421 ± 75	2.23 ± 076
9	1.66	170 ± 59	1.72 ± 0.45
10	2.24	171 ± 27	3.97 ± 0.84

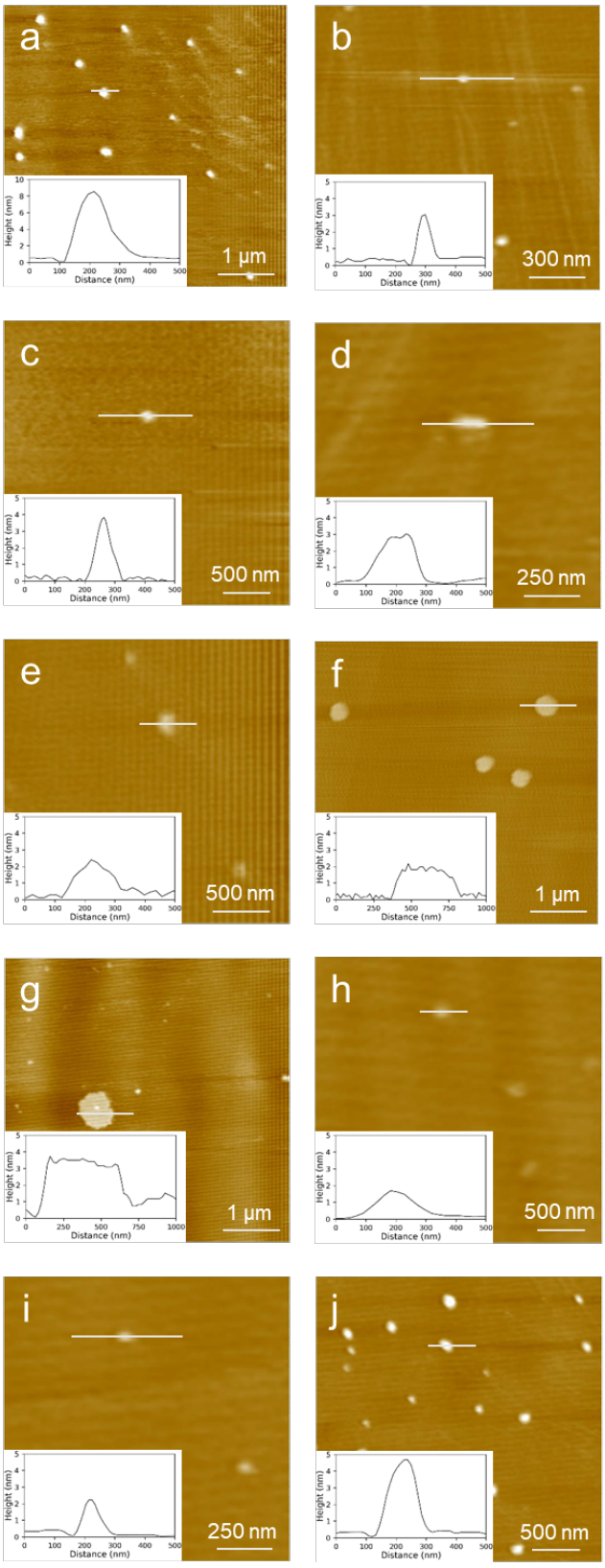

Fig. S4 AFM images and cross-sections of PdNSs. Products (a) **1**, (b) **2**, (c) **3**, (d) **4**, (e) **5**, (f) **6**, (g) **7**, (h) **8**, (i) **9**, and (j) **10** listed in Table S2.

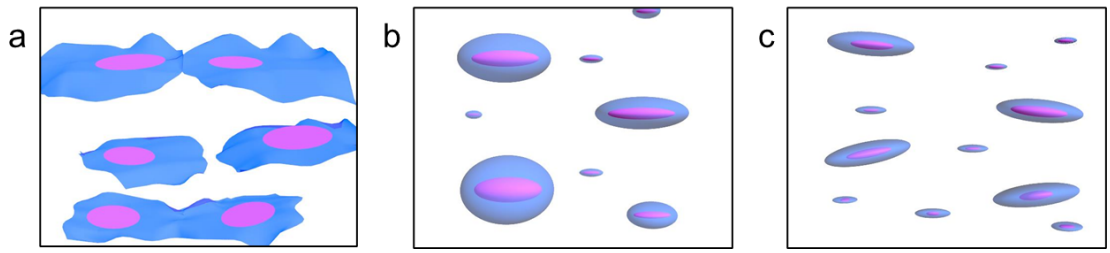

Fig. S5 Schematic illustration of the surfactant aggregates. (a) Bilayers, (b) biaxial micelles whose thickness fluctuate, and (c) mono-dispersed biaxial micelles.

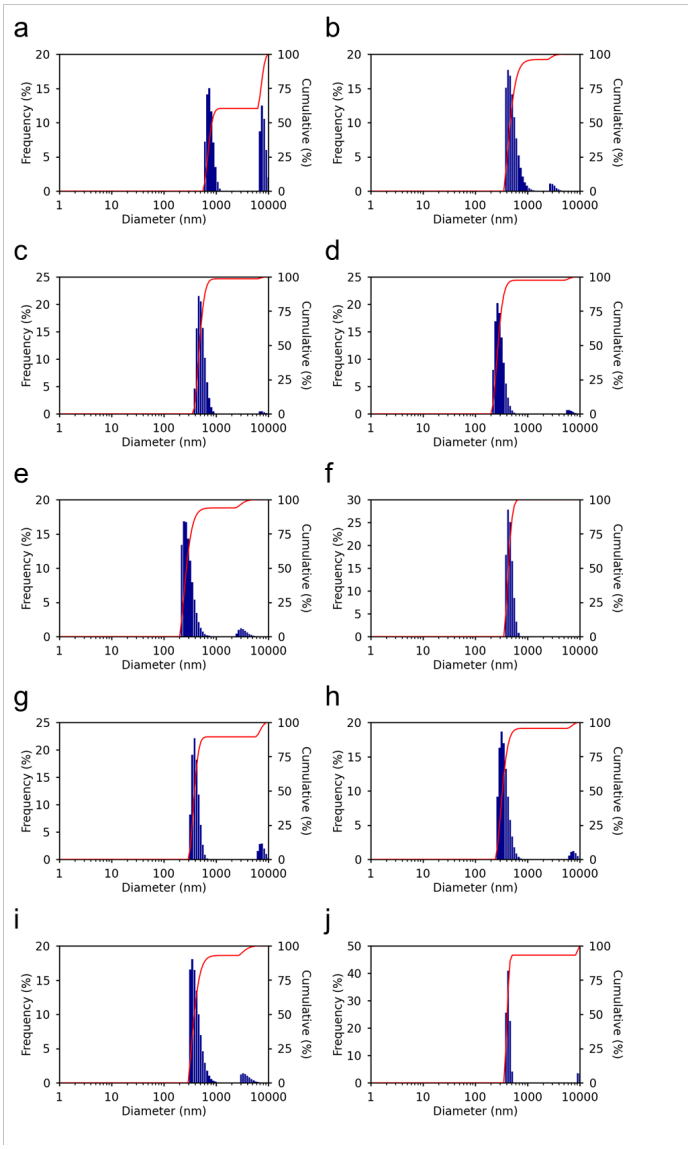

Fig. S6 Size distributions of PdNSs in the suspensions. Products (a) **1**, (b) **2**, (c) **3**, (d) **4**, (e) **5**, (f) **6**, (g) **7**, (h) **8**, (i) **9**, and (j) **10** listed in Table S2.

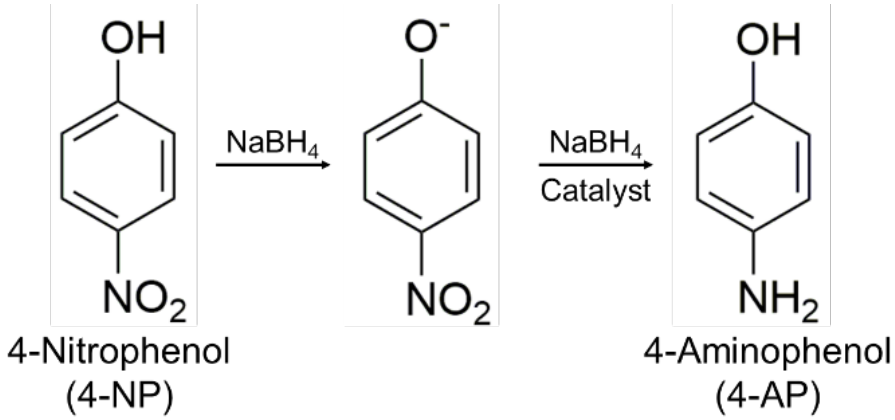

Fig. S7 Process of the conversion from 4-nitrophenol to 4-aminophenol.

Table S3 Comparison of catalytic activity for the reduction of 4-nitrophenol.

Catalyst	Pd / wt%	Size / nm	k_{app} / $s^{-1}g^{-1}$	k_{nor} / $s^{-1}g^{-1}M^{-1}$	Ref.
Pd nanosheets	100	Width: 485 ± 65 Thickness: 2.18 ± 0.40	142	28287	This study
Pd nanoparticles	100	90~410	0.39	15	S1
Pd nanoparticles	100	25	177	8992	S2
Pd nanodendrites	100	37.4 ± 5.3	98.75	1274	36
Pd/C	20	9	1366	273200	S3
Pd/CPM-2	1	70	3385	2604	S4

[a] $k_{nor} = k_{app}/(c[NaBH_4])$, where c is the total amount of the catalyst, and $[NaBH_4]$ is the borohydride concentration.

References

(S1) D. Rambabu, C. P. Pradeep, Pooja and A. Dhir, *New J. Chem.*, 2015, **39**, 8130–8135.

(S2) G. Fu, X. Jiang, L. Ding, L. Tao, Y. Chen, Y. Tang, Y. Zhou, S. Wei, J. Lin and T. Lu, *Appl. Catal. B Environ.*, 2013, **138**–**139**, 167–174.

(S3) B. Su, Y. Jia, S. Zhang, X. Chen and M. Oyama, *Chem. Lett.*, 2014, **43**, 919–921.

(S4) P. Veerakumar, R. Madhu, S.-M. Chen, V. Veeramani, C.-T. Hung, P.-H. Tang, C.-B. Wang and S.-B. Liu, *J. Mater. Chem. A*, 2014, **2**, 16015–16022.